25th ABCM International Congress of Mechanical Engineering
October 20-25, 2019, Uberlândia, MG, Brazil

COB-2019-2349
DYNAMICS OF CARDAN ACTIVE JOINTS FOR ROBOTIC APPLICATIONS

Jean C F Oliveira
Faculdade do Centro Leste (UCL), Espírito Santo, Brasil
jean@ucl.br
Hans Ingo Weber
Pontifícia Universidade Católica do Rio de Janeiro (PUC-Rio), Rio de Janeiro, Brasil
hans@puc-rio.br

Abstract.

The use of active joints is restricted by torque capacity of small motors, and embedded devices have been mandatory for robotic applications. In this paper, a new concept of robotic manipulator driven by cardan joints with three-degrees-of-freedom was introduced. Dynamic control is essential to learn the limitations of these devices, so the objective of this study is to control active cardan joints with three degrees of freedom using experimental and numerical simulations. The manipulator was designed with only one cardan joint to understand its kinematics and dynamics, for this reason, it was built with load sensors on the base and two inertial motion unit sensors, one inside the joint and the other at the top of the manipulator end factor. Furthermore, three control boards were manufactured: the first was designed to control the three stepper motor drives, the second was designed to read the inertial motion unit sensors, and the last was designed to read the load sensors. Three problem were described, but only one was developed, in which, the joint should keep the position x, y, z constant with the rotation alpha of the cardan. A new dynamic notation is introduced to clarify and simplify the mathematics used to describe the dynamics of a 3D rigid body to solve the forwards and inverse kinematics , and the numerical results from the physical model are compared with the experimental ones, to set the limits of angles and angular velocities.

Keywords: *Cardan joints, Active joints, Robotic applications*

1. INTRODUCTION

Robotic manipulators have been used not only industrially (Aspragathos et al., 2018), but also in other areas such as service (Derbel et al., 2019), medicine (Carbone et al., 2019), aerospace (Zhao et al., 2013) and so on. For this reason, one focus of this study is to adapt the robot manipulator to various uses.

In prosthetic applications, effective joints aim to simplify the several joints of the human body as three-degrees-of-freedom - 3DOF - spherical joints (Mghames et al., 2019). In surgical applications, multiple degrees-of-freedom robots are useful tools in minimally invasive surgeriesy – MIS, providing benefits, such as reduction of hand tremor, navigation, and workspace scaling (Pisla et al., 2012 and Miller et al., 2011). In aerospace applications, rocket nozzles with 3DOF (Cardoso W., 2017), or cardan mechanism for asteroid lander (38 – Zhao, 2013) may be used.

Joints are basic components of robot manipulators, which have decisive influence on their performance. The joint proposed here has 3DOF as a cardan joint. Normally, each degree-of-freedom is controlled by a motor, however, some studies involving spherical motors show it is possible to control them with only one motor (Bai et al., 2018 and Zhang et al., 2017). Nonetheless this new spherical motor is neither the focus of this study nor commercially used yet (https://aerospace.honeywell.com/spherical-motor). There are many types of joints, such as cardan or universal joints (Stamenić et al., 2012 and Krude, 1977), constant velocity kinetic joints (Cardoso W., 2018 and Krude, 1974), spherical joints (Gallardo-Alvarado et al., 2018 and Houran et al., 2018 and Froehlich et al., 2018) etc. Normally, the joints applied in robotics use external control just to obtain the position and do not consider the possibility of an internal way to transmit rotation among oblique shafts.

Active joints mean that input forces are inside the joints to control themselves, and there are many ways to do this. For example, the joint can be run by wires and cables (Yeshmukhametov et al., 2019 and Manfredi et al., 2018) or the joint can be directly driven by motors (Palpacelli et al., 2018). The mechanical challenge of using motors directly at the

rotation axis of the joint is the high torque necessary in some applications, thus the mechanical reduction is the main concern. Because of the high torque and the small scale of all components, mechanical reductions demand advanced materials, making the joint expensive. For this reason, one of the objectives of this study is to learn the limits of the applications for each kind of joint with two or three degrees of freedom.

Some related studies regarding multi-DOF joints try to reduce the number of joints and improve the output ability (Huang et al, 2017 and Shammas, 2005). When the manipulator has a lot of joints, possible mechanical gaps are accumulated leading to position errors arising from dead zones.

In this paper, a new concept of robotic manipulators driven by cardan joints with three-degrees-of-freedom is introduced. The purpose of this study is to control the dynamics and kinematics of cardan joints from the inside of the crosshead, using micro stepper motors with high-torque gearboxes to reach light and compact devices, called active joints. The active joint proposed here was designed for this study with sensors to measure its angular velocity and acceleration, and it is manufactured to make the experimental and numerical studies possible.

2. FUNDAMENTALS AND PROPOSITION

The main idea was to develop a device that would facilitate the understanding of the kinematics, dynamics, and limits of one active cardan joint. A mechanical design with sensors and control was developed to find out about the limits defining the application of the joint. During the first test, the joint will keep the position *x*, *y*, *z* (considering the inertial frame) constant under an alfa rotation of the cardan. As for the second test, the tracking path will be given throughout *x(t)*, *y(t)*, *z(t)* (considering the inertial frame) within safety zone using cardan angles (roll, pitch and yaw). In the third test, the tracking path will be given throughout *x(t)*, *y(t)*, *z(t)* (considering the inertial frame) and $\omega_O(t)$ (considering the non-inertial frame) within safety zone using cardan angles (roll, pitch and yaw), where $\omega_O(t)$ is the twist motion of the end-factor. This study will exclusively focus on the first test.

2.1 Mechanism design

The mechanism shown in Figure 1 and Figure 2 was designed using BIM (Building Information Model) methodology with the software Autodesk Inventor 2019. It was manufactured and built with a commercial cardan crosshead, motors, and reductions. The reductions attached to the crosshead are the critical parts to design the mechanism. The stepper motor is model 17HS8401 and the reduction is by planetary gearbox of 1:720 rate, made in China, which is more affordable than the gearbox and motors by Maxon, made in Switzerland.

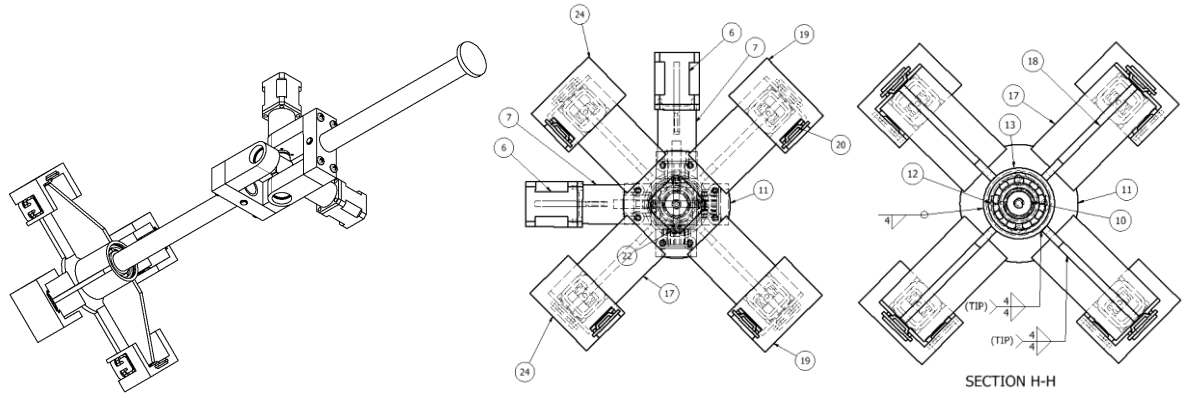

Figure 1. Isometric view (Left), Left View (Center) and Section H-H (Right) of mechanism design

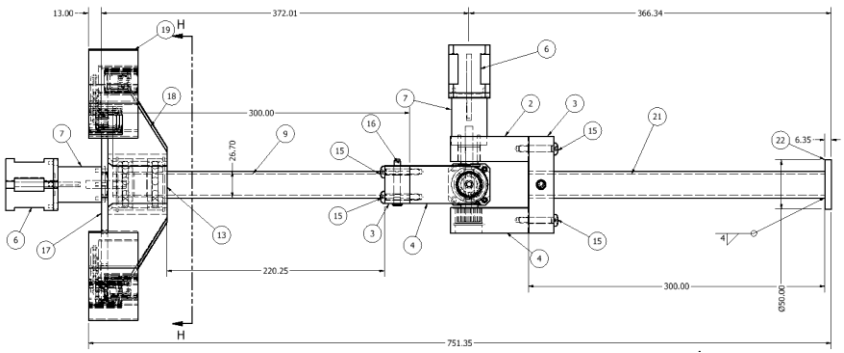

Figure 2. Front View of mechanism design

The manufacturing process and assembly were made following the good engineering practice. The Active Cardan Joint 3DOF Experiment is shown in the Figure 3.

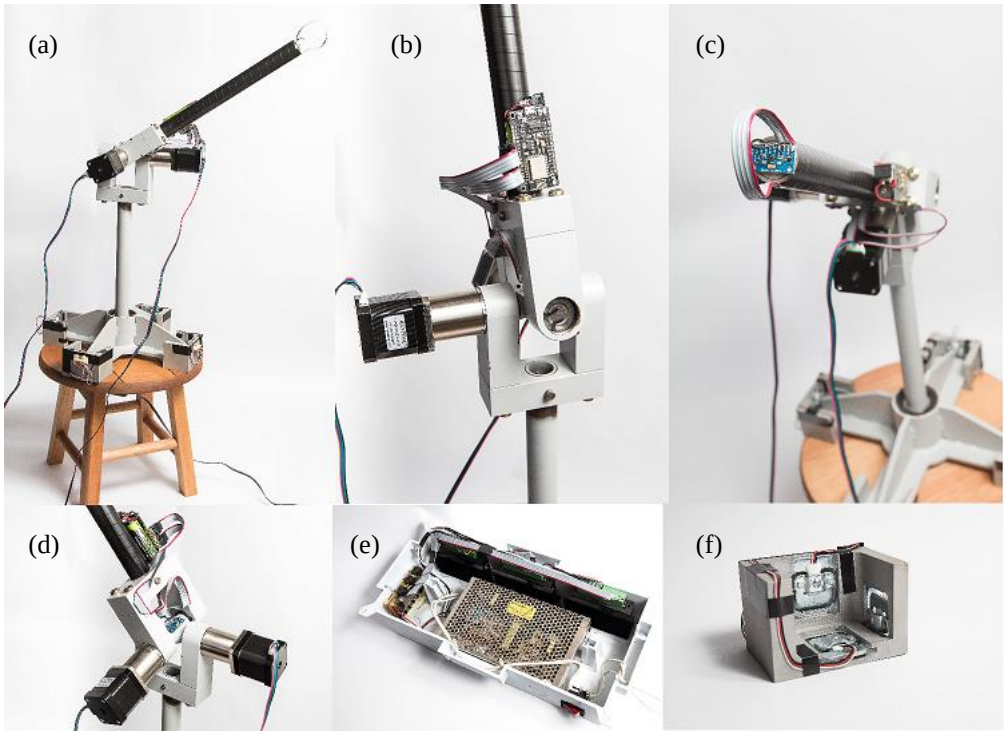

Figure 3. Active Cardan Joint 3DOF Experiment. (a) General view. (b) Joint view. (c) Manipulator end-factor view. (d) Joint view. (e) Power, Driver and Control Box. (f) Load cells support view.

2.2 Sensors and Drivers

The mechanical control uses gears and bearings as per in paper (38 – Zhao et al., 2013). However, in this study the motors are attached to the joint. The experimental procedures consist in investigating the kinematic and dynamic behavior of the manipulator robot, using an active cardan joint through path motion tracking by MPU sensors, positioned on top of the upper cylinder, and load cells to check the forces under the base support.

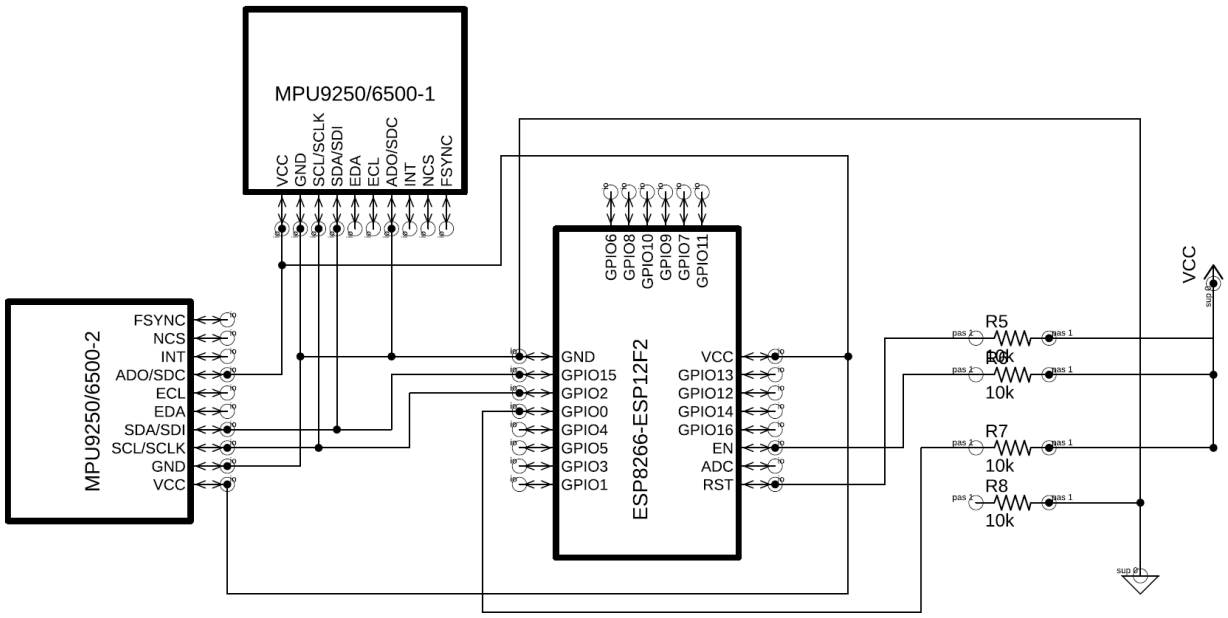

Figure 4. MPU on crosshead and MPU on upper cylinder and MPU 9250 - Schematic Diagram.

All three microcontroller shown in Figure 4, Figure 5 and Figure 6 are read by MATLAB to process the results. According to the schematic diagram in Figure 4, the sensor MPU9250 uses I2C 0x69 address and allows to get the current nine attitude values of the board, which are acceleration, gravity, and magnetic induction. At that point, MPU9250 data are read by ESP8266 microcontroller, which is a low-cost Wi-Fi microchip with full TCP/IP stack and microcontroller capability with 80 MHz and 32 bits.

Some studies (Huang et al, 2017) use computational vision to obtain the position of the end-factor manipulator. However, in this paper, the idea is to use the accelerometer to calculate the angles β and γ (pitch and yaw); hence the angle α (roll) will be given by odometry from the stepper motors under the base.

In Figure 5, schematic diagram of the load cells is shown. This weight sensor (load cell half bridge 50Kg) is suitable for electronic balance and other high accuracy electronic weighing devices. Each load cell is considered as half of one Wheatstone bridge. The other load cell was assembled to complete the bridge, instead of 1KΩ resistor, and for each bridge was assembled in 24-bit analogical-digital converter (ADC) HX711. Next, digital data from ADC HX711 are read by the other ESP8266 microcontroller. The load cell data are not shown is this paper.

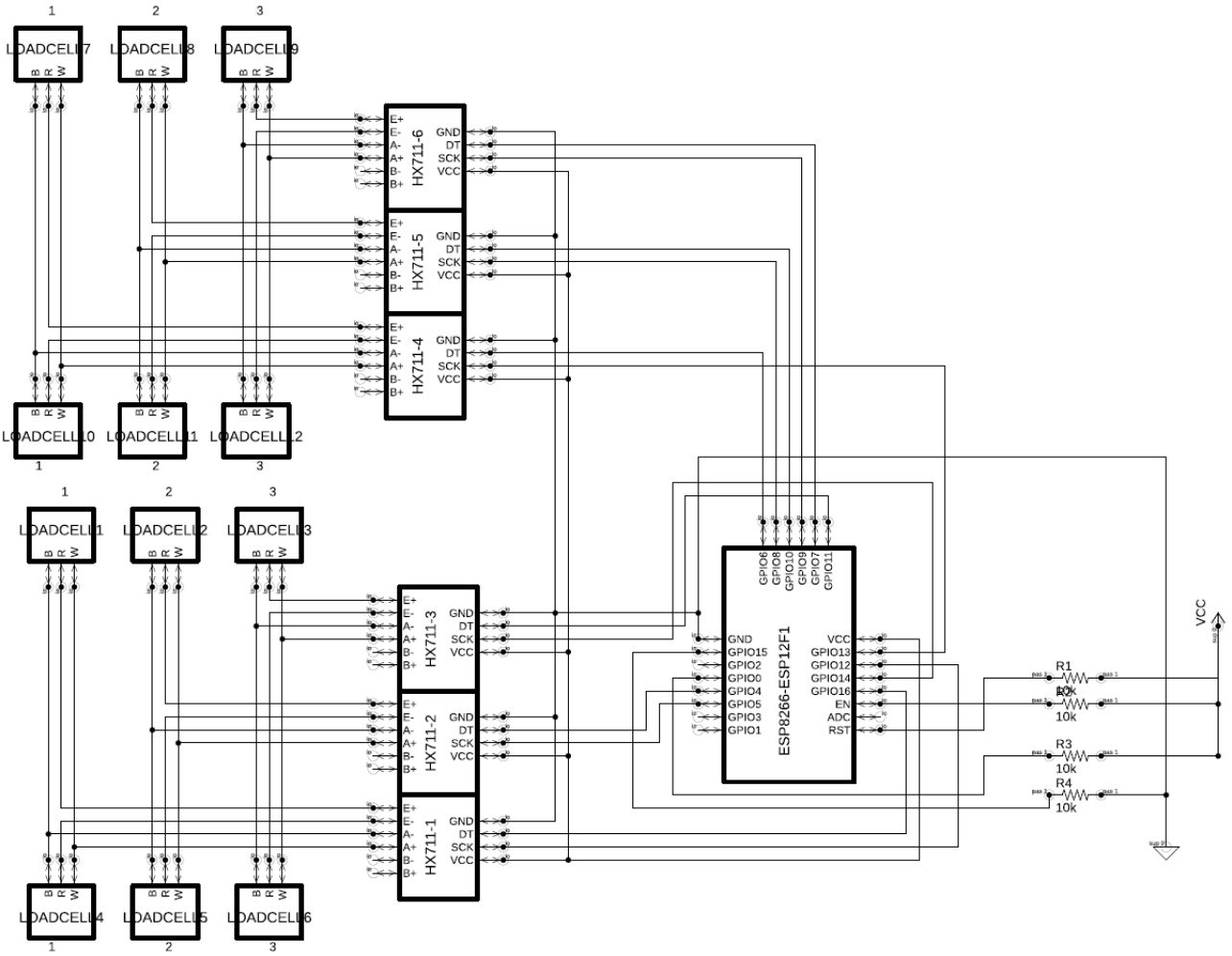

Figure 5. Support to 3 load cells, each one by axis and load cells - Schematic Diagram.

Stepper motors allow the control of the angles with pulse, if the initial position is known. In Figure 6, each stepper motor (model 17HS8401) has one microstep driver (model TB6600 – 40V – 4A) with 24 VDC supply from the power source to control the motors using the ESP-WROOM-32, which is a low-cost Wi-Fi and dual-mode Bluetooth microchip with full TCP/IP stack and microcontroller capability with 240 MHz and 32 bits.

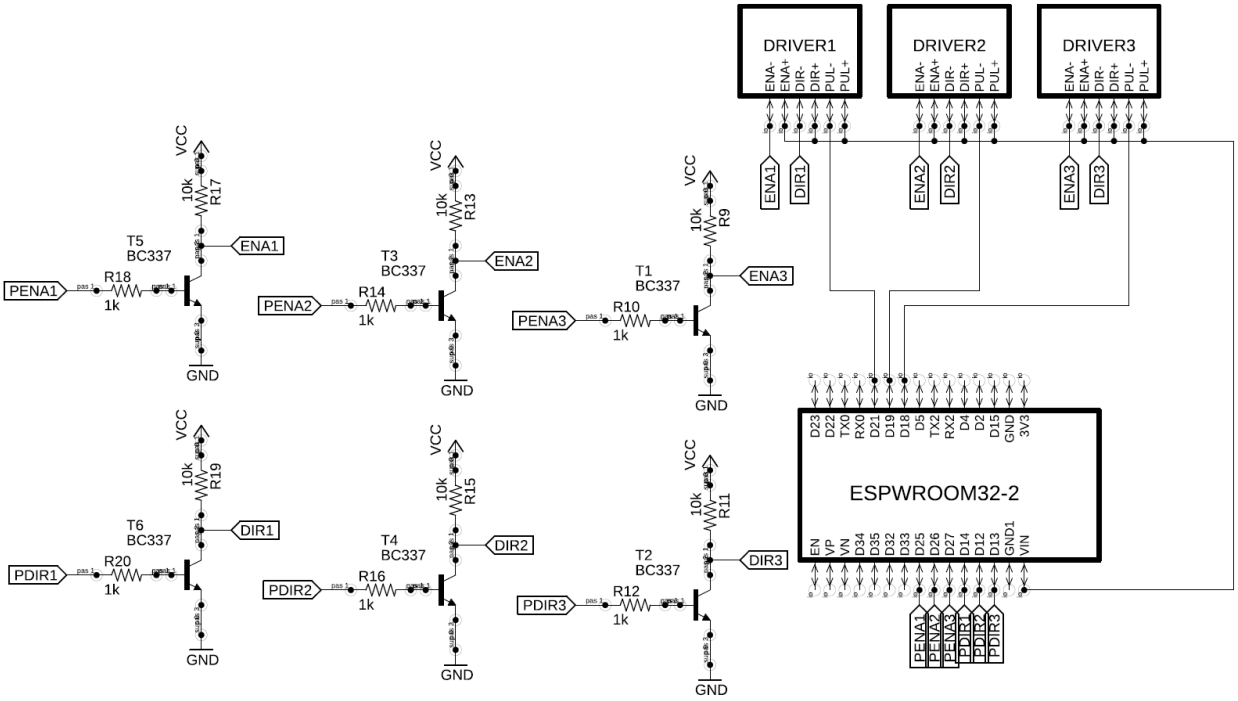

Figure 6. Box Motor Driver and its Schematic Diagram.

2.3 Kinematic Model

The first step is to model the rigid body kinematics of the experiment proposed in Figure 1, according to the current literature. However, the notation of the literature available on rigid body dynamics has issues concerning standards in the scientific community. Hence (Weber, 2019) has developed novel approach which will be applied in this study.

The frames in the experiment should be defined first to start the kinematics formulation. The frames F, Q, R, S and the angles between them are shown in Figure 7. Inside the joint, the motion produced by the two motors controls the rotation β and γ.

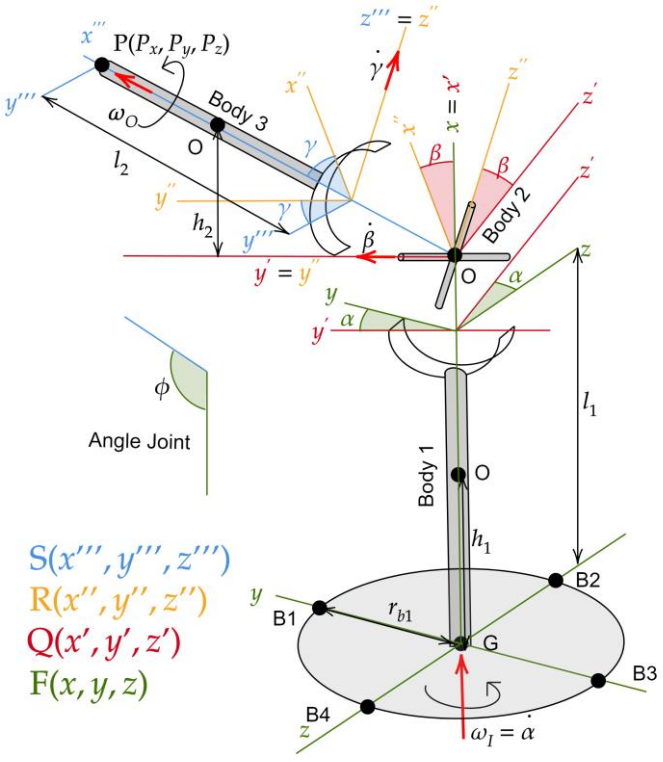

Figure 7. Universal joint and frames.

The matrix transformation according to Weber notation (Weber, 2019) is given by

$$\underset{(x,y,z)}{\mathrm{F}} \xrightarrow{\alpha\ (x)} \underset{(x,y',z')}{\mathrm{Q}} \xrightarrow{\beta\,(\mathrm{y}')} \underset{(x'',y',z'')}{\mathrm{R}} \xrightarrow{\gamma\,(\mathrm{z}'')} \underset{(x''',y''',z'')}{\mathrm{S}}$$

$$ {}^{\mathrm{F}}\mathbf{T}^{\mathrm{S}}{}_{Cardan} = {}^{\mathrm{F}}\mathbf{T}^{\mathrm{Q}}\ {}^{\mathrm{Q}}\mathbf{T}^{\mathrm{R}}\ {}^{\mathrm{R}}\mathbf{T}^{\mathrm{S}} = \begin{bmatrix} c_\beta c_\gamma & -c_\beta s_\gamma & s_\beta \\ s_\alpha s_\beta c_\gamma + c_\alpha s_\gamma & -s_\alpha s_\beta s_\gamma + c_\alpha c_\gamma & -s_\alpha c_\beta \\ -c_\alpha s_\beta c_\gamma + s_\alpha s_\gamma & c_\alpha s_\beta s_\gamma + s_\alpha c_\gamma & c_\alpha c_\beta \end{bmatrix} \tag{1}$$

In which a simplified notation was used: $\cos(\alpha) = c_\alpha$; $\sin(\alpha) = s_\alpha$; $\tan(\alpha) = t_\alpha$

The angular velocity can be written as an anti-symmetric matrix, using the time derivative of the position vector, considering its rotation matrix from Eq.(1). Back to Figure 7, "body 1" has angular velocity equal to ${}_{\mathrm{F}}\boldsymbol{\omega}_{\mathrm{Q}}$, while "body 2" has angular velocity equal to ${}_{\mathrm{F}}\boldsymbol{\omega}_{\mathrm{Q}} + {}_{\mathrm{Q}}\boldsymbol{\omega}_{\mathrm{R}}$, and "body 3" has angular velocity equal to ${}_{\mathrm{F}}\boldsymbol{\omega}_{\mathrm{Q}} + {}_{\mathrm{Q}}\boldsymbol{\omega}_{\mathrm{R}} + {}_{\mathrm{R}}\boldsymbol{\omega}_{\mathrm{S}}$.

$$ {}^{\mathrm{F}}_{\mathrm{F}}\boldsymbol{\omega}_{\mathrm{Q}} = \begin{bmatrix} \dot{\alpha} \\ 0 \\ 0 \end{bmatrix} = {}^{\mathrm{Q}}_{\mathrm{F}}\boldsymbol{\omega}_{\mathrm{Q}};\ {}^{\mathrm{Q}}_{\mathrm{Q}}\boldsymbol{\omega}_{\mathrm{R}} = \begin{bmatrix} 0 \\ \dot{\beta} \\ 0 \end{bmatrix} = {}^{\mathrm{R}}_{\mathrm{Q}}\boldsymbol{\omega}_{\mathrm{R}};\ {}^{\mathrm{R}}_{\mathrm{R}}\boldsymbol{\omega}_{\mathrm{S}} = \begin{bmatrix} 0 \\ 0 \\ \dot{\gamma} \end{bmatrix} = {}^{\mathrm{S}}_{\mathrm{R}}\boldsymbol{\omega}_{\mathrm{S}}; \tag{2}$$

"body 3":

$$ {}_{\mathrm{F}}\boldsymbol{\omega}_{\mathrm{S}} = {}_{\mathrm{F}}\boldsymbol{\omega}_{\mathrm{Q}} + {}_{\mathrm{Q}}\boldsymbol{\omega}_{\mathrm{R}} + {}_{\mathrm{R}}\boldsymbol{\omega}_{\mathrm{S}} \Rightarrow {}^{\mathrm{F}}_{\mathrm{F}}\tilde{\boldsymbol{\omega}}_{\mathrm{S}} = {}^{\mathrm{F}}\dot{\mathbf{T}}^{\mathrm{S}}\ {}^{\mathrm{S}}\mathbf{T}^{\mathrm{F}} = \begin{bmatrix} 0 & -\omega_{3z} & \omega_{3y} \\ \omega_{3z} & 0 & -\omega_{3x} \\ -\omega_{3y} & \omega_{3x} & 0 \end{bmatrix} \Rightarrow \begin{cases} \omega_{3x} = \dot{\alpha} + \dot{\gamma} s_\beta \\ \omega_{3y} = c_\alpha \dot{\beta} - c_\beta s_\alpha \dot{\gamma} \\ \omega_{3z} = s_\alpha \dot{\beta} - c_\beta c_\alpha \dot{\gamma} \end{cases} \tag{3}$$

"body 2":

$$ {}_{\mathrm{F}}\boldsymbol{\omega}_{\mathrm{R}} = {}_{\mathrm{F}}\boldsymbol{\omega}_{\mathrm{Q}} + {}_{\mathrm{Q}}\boldsymbol{\omega}_{\mathrm{R}} \Rightarrow {}^{\mathrm{F}}_{\mathrm{F}}\tilde{\boldsymbol{\omega}}_{\mathrm{R}} = {}^{\mathrm{F}}\dot{\mathbf{T}}^{\mathrm{R}}\ {}^{\mathrm{R}}\mathbf{T}^{\mathrm{F}} \Rightarrow \begin{cases} \omega_{2x} = \dot{\alpha} \\ \omega_{2y} = c_\alpha \dot{\beta} \\ \omega_{2z} = s_\alpha \dot{\beta} \end{cases} \tag{4}$$

"body 1":

$$ {}_{\mathrm{F}}\boldsymbol{\omega}_{\mathrm{Q}} = {}_{\mathrm{F}}\boldsymbol{\omega}_{\mathrm{Q}} \Rightarrow {}^{\mathrm{F}}_{\mathrm{F}}\tilde{\boldsymbol{\omega}}_{\mathrm{Q}} = {}^{\mathrm{F}}\dot{\mathbf{T}}^{\mathrm{Q}}\ {}^{\mathrm{Q}}\mathbf{T}^{\mathrm{F}} \Rightarrow \begin{cases} \omega_{1x} = \dot{\alpha} \\ \omega_{1y} = 0 \\ \omega_{1z} = 0 \end{cases} \tag{5}$$

There is a phase shift in the Cardan joint between the angular velocities of the shafts that depend on the angle ϕ between the links. It can be calculated as shown in (Weber, 2019)

$$\begin{aligned} \phi &= \arccos(c_\beta c_\gamma) \\ \omega_O &= \frac{\omega_I}{c_\phi + s^2{}_\alpha s_\phi t_\phi} \end{aligned} \tag{6}$$

To develop the forward and inverse kinematics, the position at point P in frame F can be written by:

$$ {}^{\mathrm{F}}_{\mathrm{G}}\mathbf{r}_{\mathrm{P}} = {}^{\mathrm{F}}_{\mathrm{G}}\mathbf{r}_{\mathrm{O}_2} + {}^{\mathrm{F}}\mathbf{T}^{\mathrm{S}}\ {}^{\mathrm{S}}_{\mathrm{O}_2}\mathbf{r}_{\mathrm{P}} = \begin{bmatrix} l_1 \\ 0 \\ 0 \end{bmatrix} + \begin{bmatrix} c_\beta c_\gamma & -c_\beta s_\gamma & s_\beta \\ s_\alpha s_\beta c_\gamma + c_\alpha s_\gamma & -s_\alpha s_\beta s_\gamma + c_\alpha c_\gamma & -s_\alpha c_\beta \\ -c_\alpha s_\beta c_\gamma + s_\alpha s_\gamma & c_\alpha s_\beta s_\gamma + s_\alpha c_\gamma & c_\alpha c_\beta \end{bmatrix} \begin{bmatrix} l_2 \\ 0 \\ 0 \end{bmatrix} = \begin{bmatrix} P_x \\ P_y \\ P_z \end{bmatrix} \tag{7}$$

$$ \begin{bmatrix} P_x \\ P_y \\ P_z \end{bmatrix} = \begin{bmatrix} l_1 + l_2 c_\beta c_\gamma \\ l_2 (c_\alpha s_\gamma + s_\alpha s_\beta c_\gamma) \\ l_2 (s_\alpha s_\gamma - c_\alpha s_\beta c_\gamma) \end{bmatrix} \tag{8}$$

The general solution of the inverse kinematics is not solved analytically. However, to solve problem 1 proposed, α angle can be determined because of the constant angular velocity ω_1, $\alpha = \omega_1 t$. The analytical solution for "problem 1" is shown in Figure 9 (top left). As for "problem 2", if the tracking path is inside the safety zone, α angle could be zero ($\alpha = 0$). To operate the joint outside the safety zone, α angle must be constant ($\alpha = cte$) to keep the experiment inside the limit of the joint. As for "problem 3", α angle is an input as a continuum function on the time ($\alpha(t)$), and the joint must operate exclusively inside the safety zone consequently. Thus, the β and γ angles are given by the equations below:

$$\gamma = \arcsin\left(\frac{P_y}{l_2}c_\alpha + \frac{P_z}{l_2}s_\alpha\right);\ \beta = \arccos\left(\frac{P_x - l_1}{l_2 c_\gamma}\right) \tag{9}$$

Thus, all the motion of the three bodies is learned, using forward kinematics and inverse kinematics to solve the problems proposed with the manipulator robot.

3. RESULTS

3.1 Angles Limits - Workspace

Generally, high torque in the reduction is a critical condition for active joints, and it is important to obtain the joint limits to protect it from the contact. Any contact at any point of the joint could break it. To measure the limits, first the motors were removed and the joint was operated manually until the limit is reached. Second, the motors were assembled, and the joint was operated manually until the limit is reached again. By analyzing the end-factor accelerometer, it is possible to calculate the angles, as shown below:

$$\begin{aligned} \beta &= a\tan 2(a_x, \sqrt{a_y{}^2 + a_z{}^2}) \\ \gamma &= a\tan 2(a_y, \sqrt{a_x{}^2 + a_z{}^2}) \end{aligned} \tag{10}$$

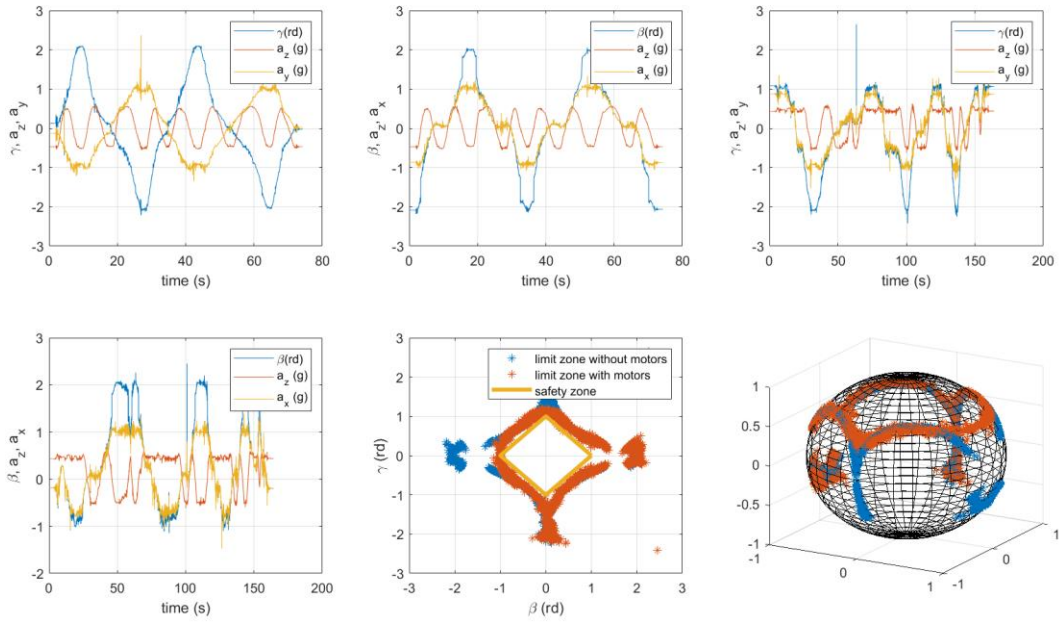

Figure 8 - Accelerometer a_z, a_y and γ without motors (top-left), accelerometer a_z, a_x and β without motors (top-middle), accelerometer a_z, a_y and γ with motors (top-right), accelerometer a_z, a_x and β with motors (bottom-right), zone β x γ (bottom-middle) and spherical motion of the end-factor (bottom-right).

The safety zone was determined analyzing Figure 8, and the motor odometry was limited inside this zone to ensure the safe operation of the active joint. In this case, the rhombus of 1 radian was adopted. Angles β and γ can be

improved if the accelerometer, gyroscope, and magnetometer are used as input. Some inconsistency is found in the regions of instability, because of the trigonometric behavior.

3.2 Problem 1

In this problem, the joint should keep the position x, y, z constant with the rotation alpha of the cardan. The alpha angular velocity of $\omega_1 = 0.2\ rad/s$ was adopted, and the other angles can be calculated by Eq. (9) or Eq. (11), according to (Weber, 2019).

$$\beta = \arctan(t_\phi s_\alpha)$$
$$\gamma = \arctan(s_\beta / t_\alpha) \tag{11}$$

The IMU (Inertial Measurement Unit) positioned on the end-factor manipulator is not sensitive to alpha angle. For this reason, alpha value will be adopted from alpha stepper motor odometry. In Figure 9 (top-left), a small difference between analytic solution and experimental solution using odometry of motors alpha, beta and gamma is shown. In Figure 9 (top-middle) and in Figure 9 (top-right), the comparison between β and γ angles from IMU and Odometry is shown, and it is possible to see the IMU variation when β and γ angles change the rotation sense due to the slack. Other data to be observed is the pseudo circular motion in Figure 9 (bottom-left) and Figure 9 (bottom-right). Due to the twist in the upper stem, the motion of beta motor and gamma motor is the same, when the alpha motor is stalled, and the tracking path makes a circle on the spherical workspace.

Once angles α, β and γ are learned at that given time, it is possible to calculate the bodies' kinematics from Eq. (3), Eq. (4) and Eq.(5). In Figure 10 (top-left), a comparison between the constant velocity ($\omega_{1x} = \dot{\alpha}$) of the experiment results and analytic results related to "body 1" is shown, which behaved as expected. In Figure 10 (top-right), the comparison was satisfactory, but it is possible to see the shift of phase among the graphs. It occurs because the offset of time was set manually. The kinematics of "body 2" has all the three components of angular velocity, but the kinematics of "body 3" has only two of three components of angular velocity, as shown in Figure 10 (bottom).

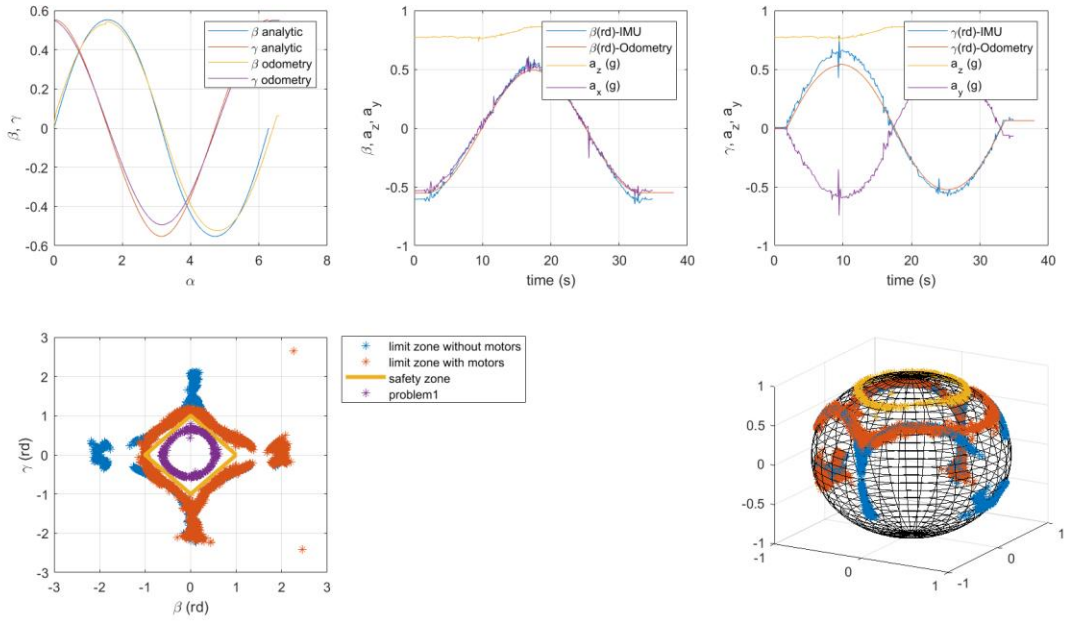

Figure 9. Comparison between analytical solution and experimental solution (top-left), accelerometer a_z, a_y and β beta by IMU and Odometry to problem1(top-middle), accelerometer a_z, a_x and γ gamma by IMU and Odometry to problem 1 (top-right), zone β x γ (bottom-left) and spherical motion of the end-factor to problem 1 (bottom-right).

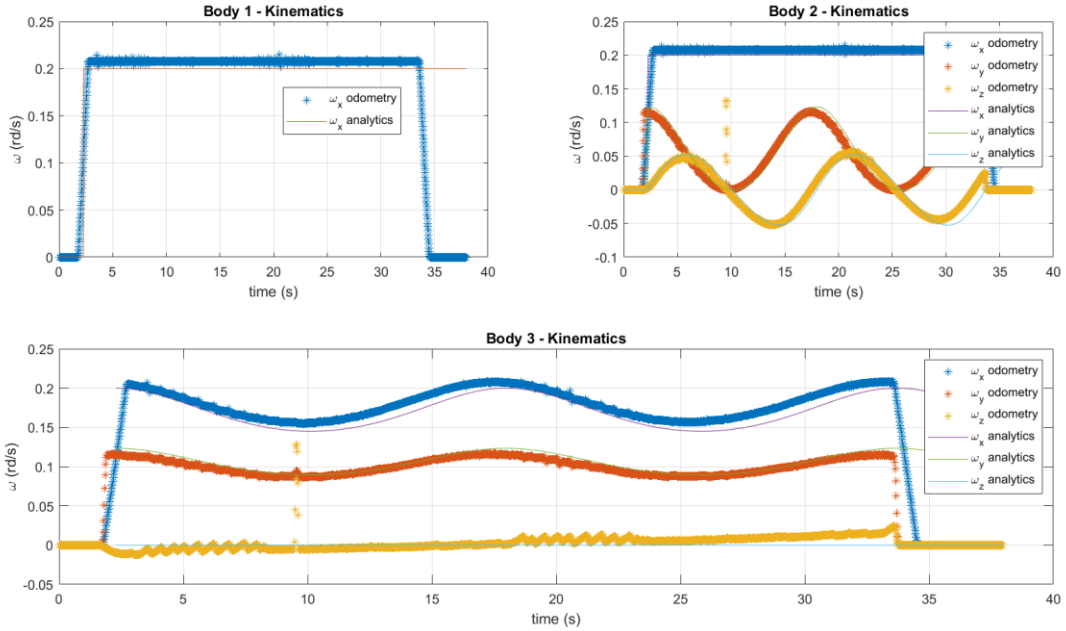

Figure 10. Comparison between analytical solution and experimental solution of the angular velocities of rigid bodies.

4. CONCLUSION

The experiment of the active cardan joint created to show the limits of performance and the principle of its kinematics achieved satisfactory results to start with the dynamic studies. For small velocities, the kinematics behaved as expected, very close to the analytical result. However, some improvements need to be made in the experiment so as to get a better accuracy in the results, since the velocities involved are intended to be increased, which will make its dynamics more interesting. These improvements shall be proposed in a future study, and it will consist of reducing the joint slack, improving the readings of the IMUs, and monitoring the forces and torques. Therefore, the focus of this study was to validate the kinematics of the proposed problems, particularly "problem 1" in this case, so as to study the dynamics in the future.

The major share of the joint gap occurs between the reducer shaft and the hub, due to imprecision in the manufacturing process. The gap always occurs when there is change in the sense of rotation of the shaft. So, a coupling between the shaft and the hub through a threaded orifice between them will be proposed, thereby ensuring that no relative movement of rotation between them occurs.

In this study, only the readings of the accelerometers of the IMUs were used without applying any type of filter. The reading taking into account the measurements of the accelerometers, gyroscope and magnetometer passing through an extended Kalman filter will be proposed as an improvement aiming to increase the reliability and accuracy of the results.

5. REFERENCES

Akpolat Zuhtu Hakan, Bingol M. C., Ay M., Koca O. G., Bal C and Korkmaz D.. 2017. “Dynamic model and simulation of one active joint robotic fish”. *Enginering Sciences – NWSAENS*, 1A0370, pp 29-39.

Aspragathos Nikos A., Koustoumpardis Panagiotis N., Moulianitis Vassilis C. 2018. “Advances in Service and Industrial Robotics: Proceedings of the 27th International Conference on Robotics in Alpe-Adria Danube Region (RAAD 2018)”. Springer - Advances in Service and Industrial Robotics: Proceedings of the 27th International Conference on Robotics.

Bai Kun, Xu Ruoyu, Lee Kok-Meng, Dai Wang, Huang YongAn. 2018. “Design and Development of a Spherical Motor for Conformal Printing of Curved Electronics”. IEEE Transactions On Industrial Electronics.

Carbone Giuseppe, Ceccarelli Marco, DoinaPisla. 2019. “New Trends in Medical and Service Robotics: Advances in Theory and Practice”. Springer - Mechanisms and Machine Science.

Cardozo W. S., 2017. Numerical ans experimental study of a two degrees of freedom electrohydraulic manipulator. Thesis, Pontifícia Universidade Católica, Rio de Janeiro, Brasil.

Cardozo William Schroeder, Weber Hans Ingo. 2018. "A compact formulation for constant velocity joint kinematics". Mechanism and Machine Theory. Volume 121, March 2018, Pages 1-14.

Derbel Nabil, Ghommam Jawhar, QuanminZhu. 2019. "New Developments and Advances in Robot Control". Springer - Studies in Systems, Decision and Control.

Gallardo-Alvarado Jaime, Rodriguez-Castro Ramon, Perez-Gonzalez Luciano, Aguilar-Najera Carlos R. 2018. "Kinematics of the 3(RPSP)-S Fully Spherical Parallel Manipulator by Means of Screw Theory". A special issue of Robotics (ISSN 2218-6581).

Huang He, Dong Erbao, Xu Min, Yang Jie, Low Kin Huat. 2017. "Mechanism design and kinematic analysis of a robotic manipulator driven by joints with two degrees of freedom (DOF)". The International Journal Of Robotics Research And Application Volume 45, Issue.

Froehlich Tim, Reiser Ulrich, Meßmer Felix, Verl Ing. Alexander. 2018. "Concept and Design of a Spherical Joint Mechanism for Service Robots". Procedia Manufacturing Volume 24, 2018, Pages 74-79.

Houran Mohamad Abou, Yang Xu, Chen Wenjie. 2018. "Free Angular-Positioning Wireless Power Transfer Using a Spherical Joint". A special issue of Energies (ISSN 1996-1073).

Krude Werner. 1977. "Angularly flexible cardan shaft joint". https://patents.google.com/patent/US4156354A.

Krude Werner. 1974. "Constant velocity torque transmitting joint". https://patents.google.com/patent/US4012925A.

Manfredi Luigi, Alfred Cuschieri. 2018. "Design of a 2 DOFs Mini Hollow Joint Actuated with SMA Wires". Materials (Basel, Switzerland), ISSN: 1996-1944, Vol: 11, Issue: 10, Page: 2014

Miller Laura A., Lipschutz Robert D., Stubblefield Kathy A., Lock Blair A., Huang He, Williams III T. Walley, Weir Richard F., Kuiken Todd A. 2011. "Control of a Six Degree-of-Freedom Prosthetic Arm after Targeted Muscle Reinnervation Surgery". Arch Phys Med Rehabil. 2008 Nov; 89(11): 2057–2065.

Mghames Sariah, Catalano Manuel G., Bicchi Antonio and Grioli Giorgio, 2019. "A Spherical Active Joint for Humanoids and Humans". *IEEE Robotics and Automation Letters*, Vol. 4, No. 2, pp. 838-845.

Palpacelli Matteo, Carbonari Luca, Palmieri Giacomo, Callegari Massimo. 2018. "Design of a Lockable Spherical Joint for a Reconfigurable 3-URU Parallel Platform". Kinematics and Robot Design I, KaRD2018.

Pisla Doina, Gherman Bogdan, Vaida Calin, Plitea Nicolae. 2012. "Kinematic modelling of a 5-DOF hybrid parallel robot for laparoscopic surgery". Robotica (2012) volume 30, pp. 1095–1107. © Cambridge University Press 2012.

Weber, Hans Ingo. 2019. *Raciocinando Dinâmica de Rotação – Bases para o entendimento de rotação – Dinâmica de Rotação de Corpo Rígido, Cinemática Tridimensional*. Vol 1, Amazon KDP – Kindle Direct Publishing, 1st edition.

Shah S. V., Saha S. K., Dutt J. K. 2012. "Denavit-Hartenberg Parameterization of Euler Angles". Journal of Computational and Nonlinear Dynamics April 2012, Vol. 7 / 021006-1 ASME.

Shammas Elie, Wolf Alon, Chose Howie. 2005. "Three degrees-of-freedom joint for spatial hyper-redundant robots". Mechanism and Machine Theory. Volume 41, Issue 2, February 2006, Pages 170-190.

Stamenic Z, Ristivojevic M, Tasic M and Mitrovic R, 2012. "Influence of the Geometry Parameters of Cardan Joint Rolling Parts on the Load Distribution". *FME Transactions*, Vol 40, No 3, pp. 135-143.

Yeshmukhametov Azamat, Koganezawa Koichi and Yamamoto Yoshio. 2019. "Design and Kinematics of Cable-Driven Continuum Robot Arm with Universal Joint Backbone". *IEEE International Conference on Robotics and Biomimetics*, December 12-15, 2018, Kuala Lumpur, Malaysia, pp 2444-2449.

Zhang Fan, Zeng Li, Zhu Zhi-Da and Sun Jin, 2017. "Electromagnetics Driving Modal and Control of Magnetic Levitation Spherical Active Joint". 3rd *Annual International Conference on Mechanics and Mechanical Enginreering*, Advances in Engineering Research – AER, Vol 105, pp 763-772.

Zhao Zhijun, Zhao Jingdong, Liu Hong, Zhang Zhi, 2013. "Development of a Cardan Mechanism for the Asteroid Lander". *International Journal on Smart Sensing and Intelligent System*, Vol. 6, No 3, pp. 1283-1297.

6. RESPONSIBILITY NOTICE

The authors are the only accountable for the printed material included in this paper.